JOURNAL OF QUATERNARY SCIENCE (2020) **35**(1-2) 175–185 ISSN 0267-8179. DOI: 10.1002/jqs.3152

JQS Journal of Quaternary Science QRA Quaternary Research Association

The importance of grain size and shape in controlling the dispersion of the Vedde cryptotephra

JENNIFER SAXBY,[1]* KATHARINE CASHMAN,[2] ALISON RUST[2] and FRANCES BECKETT[3]
[1]School of Earth Sciences, University of Bristol Wills Memorial Building Queens Road, Bristol, BS8 1RJ, UK
[2]Dept. Earth Sciences, University of Bristol, Queen's Road, Bristol, BS8 1RJ, UK
[3]Met Office, FitzRoy Road, Exeter, EX1 3PB, UK

Received 31 March 2019; Revised 10 September 2019; Accepted 17 September 2019

ABSTRACT: Volcanic ash is dispersed in the atmosphere according to meteorology and particle properties, including size and shape. However, the multiple definitions of size and shape for non-spherical particles affect our ability to use physical particle properties to understand tephra transport. Moreover, although particles >100 μm are often excluded from operational ash dispersion model setups, ash in tephra deposits > 1000 km from source can exceed 100 μm. Here we measure the shape and size of samples of Vedde ash from Iceland, an exceptionally widespread tephra layer in Europe, collected in Iceland and Norway. Using X-ray computed tomography and optical microscopy, we show that distal ash is more anisotropic than proximate ash, suggesting that shape exerts an important control on tephra dispersion. Shape also impacts particle size measurements. Particle long axis, a parameter often reported by tephrochronologists, is on average 2.4× greater than geometric size, used by dispersion modellers. By using geometric size and quantifying shape, we can explain the transport of Vedde ash particles ≤190 μm more than 1200 km from source. We define a set of best practices for measuring the size and shape of cryptotephra shards and discuss the benefits and limitations of using physical particle properties to understand cryptotephra transport. © 2019 Crown copyright. *Journal of Quaternary Science* Published by John Wiley & Sons Ltd.

KEYWORDS: volcanic ash; dispersion modelling; cryptotephra deposits; particle shape; settling velocity.

Introduction

The ejection of fine ash [defined by Rose and Durant (2009) as diameters <1000 μm, which fall in the intermediate flow regime] into the atmosphere from large volcanic eruptions can result in widespread dispersal of tephra. Distal ash deposits (here > 1000 km from source) are often preserved as non-visible (crypto-) tephra layers comprising low concentrations of ash shards preserved in peat or lake sediments or ice cores. Shards can be identified by their characteristic translucent glassy appearance and bubbly or platy morphologies and are linked to tectonic regions or specific volcanoes by geochemical analysis (Tomlinson *et al.*, 2015). By linking the ash to an eruption of known age, cryptotephra deposits provide continental-scale age frameworks for their host sediment sequences. Cryptotephra studies can also improve understanding of volcanic processes, constrain eruptive histories (Wastegård, 2002; Lawson *et al.*, 2012) and, when combined with dispersion modelling, be used to assess past atmospheric conditions (Lacasse, 2001; Lacasse and van den Bogaard, 2002) and ash transport mechanisms (Stevenson *et al.*, 2010, 2013, 2015; Watson *et al.*, 2016; Dunbar *et al.*, 2017). When particle size distributions (PSDs) and ash shard concentrations are reported, these data can improve constraints on total eruptive volumes, which are usually only calculated from proximal tephra (Ponomareva *et al.*, 2015).

*Correspondence: Jennifer Saxby, School of Earth Sciences, University of Bristol Wills Memorial Building Queens Road Bristol, UK BS8 1RJ.
E-mail: jennifer.saxby@bristol.ac.uk

Many cryptotephra layers originating from Iceland can be found in northern Europe (Lawson *et al.*, 2012); these distal deposits provide a valuable record of eruptions in Iceland during the Quaternary, for which proximal deposits are scarce due to glaciation (Lane *et al.*, 2012). However, dispersion modellers have been unable to account for the travel distances of the largest grains (typically >80 μm) in such deposits (Lacasse, 2001; Beckett *et al.*, 2015; Stevenson *et al.*, 2015; Watson *et al.*, 2016). Numerical models show that dispersion distance is sensitive to particle size and shape for cryptotephra-sized grains (Beckett *et al.*, 2015; Saxby *et al.*, 2018). Cryptotephra studies often report size as maximum grain length L (the greatest distance between two parallel tangents on the grain), and do not report shape, while models use the geometric size d_v (diameter of a volume-equivalent sphere) and can include a shape parameter. For very non-spherical particles, L and d_v can differ significantly (Saxby *et al.*, 2018).

We explore here whether particle shape is one of the contributing factors in long-distance ash transport, using proximal and distal samples of the 12.1 ka BP Vedde tephra from Katla volcano, Iceland. We quantify the shape and size of ash shards and use these data to model their transport. We show that by quantifying geometric size and particle shape, we can explain the dispersion of the largest shards (<191 μm) of the Vedde tephra to sites in Norway, a distance of > 1200 km, given a plume height of > 20 km above ground level (agl). Travel distance is sensitive to particle shape, and the method of size measurement; we can only account for the significant travel distance of some large cryptotephra shards by using consistent size and shape parameters from measurement to modelling. We also assess different measures of particle size

and determine the dependence of shard size on the amount of material sampled.

Particle shape and tephra transport

Far from the vent, where the influence of plume dynamics is negligible, volcanic ash dispersion is controlled by meteorological conditions (e.g. wind advection and turbulent diffusion) and the sedimentation velocity of the particles. In dry conditions, sedimentation velocity is controlled by terminal fall velocity, which is sensitive to air density, air viscosity, and particle size, shape and density (Folch, 2012; Beckett *et al.*, 2015). Non-spherical volcanic ash particles have a lower terminal velocity than equivalent-volume spheres (Riley *et al.*, 2003). Therefore, to understand the dispersion of cryptotephra it is essential to constrain particle properties. The influence of shape on cryptotephra dispersion distance, however, has not been examined.

Cryptotephra are typically characterized by ash grains of $L = 25 - 80$ μm (Blockley *et al.*, 2005). However, grain size is not often reported. Where sizes are given, they are often modal or maximum sizes, and the amount of material required to accurately constrain these parameters is unclear. In addition, the process of extracting cryptotephra from sediment often involves the mechanical removal of larger and/or smaller sediment particles by sieving (e.g. Turney, 1998; Blockley *et al.*, 2005), limiting the range of observed sizes. Descriptions of cryptotephra morphology are often qualitative, with ash particles characterized by glassy bubble wall fragments with winged, platy or fluted morphologies (e.g. Mangerud *et al.*, 1984; Stevenson *et al.*, 2013). Although this suggests a link between ash morphology and distal transport, shape measurements are scarce, and where given, are often ratios between particle axis lengths measured in 2D (e.g. Watson *et al.*, 2016). Shape-dependent particle terminal velocity equations used in dispersion models, in contrast, are calibrated using 3D shape measures (e.g. Wilson and Huang, 1979; Ganser, 1993; Bagheri and Bonadonna, 2016). By measuring the 3D shape of distal tephra particles we can better determine the sensitivity of travel distance to particle shape using dispersion modelling.

The Vedde ash

The Vedde ash, dated to 12.1 ka BP (Rasmussen *et al.*, 2007), is an exceptionally widespread event horizon that is described in > 60 terrestrial and ice sequences and > 30 marine deposits throughout Europe and the north Atlantic, as distally as the Ural Mountains, Siberia (Haflidason *et al.*, 2018), making it an important marker for the correlation of Quaternary sequences (Lane *et al.*, 2012). Few proximal outcrops are described, probably due to the extensive glaciation of Iceland during the Younger Dryas at 12.6-12.0 ka BP (Ingólfsson and Norðdahl, 2010). The Vedde ash, with a bimodal composition (45-58% and 72-76% SiO_2), has been geochemically linked to Katla volcano, Iceland (Mangerud *et al.*, 1984). Distally it is characterized by cuspate, winged or platy shards (Fig. 1) interpreted as thin bubble wall structures (Norðdahl and Haflidason, 1992). It is unclear to what extent these particle shapes have influenced distal transport.

Although the Vedde ash mostly occurs as cryptotephra, there are several lake and peat bog sites in the Ålesund and Nordfjord areas of western Norway (Fig. 2, inset) with exceptionally thick (≤50 cm) deposits, created by drainage into palaeolakes from larger catchment areas (Mangerud *et al.*, 1984). We examine six Vedde ash samples from visible deposits (thickness 0.5-21 cm) in Norway as well as one proximal sample from Iceland (Fig. 2; Table 1). The deposits provide large sample sizes, allowing us to accurately quantify maximum and modal shard size and determine the number of shards necessary for accurate measurement. The reworked ash in Norway is in both marine and lacustrine sediments, ruling out ocean circulation or ice rafting as a transport mechanism (Mangerud *et al.*, 1984), and so we can assume the ash was transported to the lake catchments by atmospheric circulation. The distance over which the ash has been transported after deposition is therefore negligible compared to the distance it was transported before deposition.

Methods

Determining particle size, shape and density

We sieved all samples at half-φ intervals, apart from sample KV5 which was sieved to >62.5 μm prior to this study. We manually picked ~ 10 of the largest ash shards from each Norwegian sample and mounted them on tape with maximum projected area in view. Maximum projected area A_{max}, perimeter P and maximum axis length L were obtained through optical microscopy images analysed with ImageJ software. Grain depth D was estimated by focusing down through the translucent particles using a dial with increments of 1 μm; we estimated volume by $V = A_{max} D$ and surface area by $A_{surf} = 2A_{max} + PD$. This approximation does not consider surface roughness, which is a reasonable simplification as the particles examined are smooth-sided bubble wall shards. We calculated sphericity as a function of volume and surface area:

$$\psi = \frac{\pi^{\frac{1}{3}}(6V)^{\frac{2}{3}}}{A_{surf}} \quad (1)$$

(Ganser, 1993). With this definition, a sphere has $\psi = 1$ and the value decreases towards zero with increasing difference from a spherical shape; for example, an oblate spheroid with a ratio between semi-major and semi-minor axes of 2:1 has a sphericity of 0.91. We obtained d_v by solving for the diameter of a volume-equivalent sphere. We averaged the five particles with the largest d_v as representative of maximum d_v (d_{v5}) and L (L_5) for each sample.

To obtain bulk shape descriptors, and determine the impact of sample size on measurements, we also scanned > 300 particles from the $62.5 - 125$ μm ($3 - 4$ φ) sieve fraction of each sample, using X-ray microcomputed tomography (CT). We used a single size fraction, where the proximal and distal PSDs overlap, as particle shape can be size-dependent (e.g. Mele and Dioguardi, 2018). To separate particles, we encased them in epoxy resin within 6-mm-diameter, 20-mm-long plastic cylinders. X-ray projections were taken as the cylinders were rotated 360°. The resolution of 3.5 μm voxel edge length gave > 2800 voxels/particle; a minimum of 1200 voxels/particle gives an

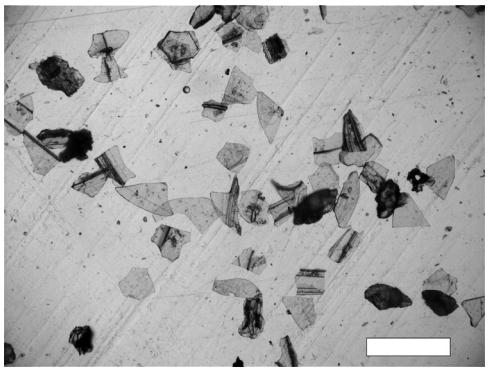

Figure 1. Vedde ash shards from western Norway (sample KV1); $125 - 180$ μm sieve fraction. Scale bar = 500 μm.

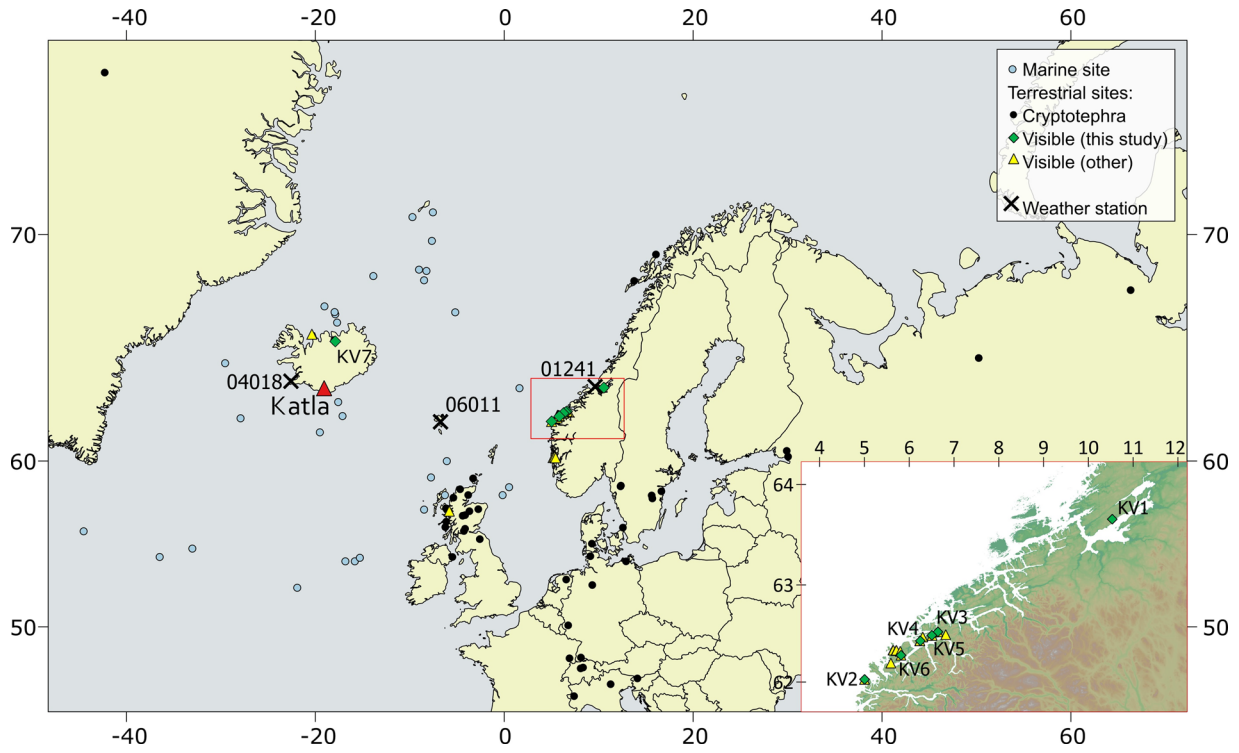

Figure 2. Documented occurrences of the Vedde ash in terrestrial and marine sites. All data sources are given in the Supporting Information. Sites labelled KV are the source of samples described in this study. Area in red is enlarged in the inset to show locations of samples from Norway. Numbered black crosses denote weather stations in the North Atlantic region from which we analyse wind velocity data. [Color figure can be viewed at wileyonlinelibrary.com].

accurate mean ψ (Saxby *et al.*, 2018). A 3D volume, constructed from 2D image slices using CT Pro 3D, allowed segmentation of the particles from the much less dense epoxy according to greyscale values, and the surfaces of the particles were reconstructed with Avizo software. We employed the Label Analysis module to calculate V, A_{surf}, and the three principal axis lengths L, I, and S (long, intermediate and short axes, respectively) of each particle. Using these axis lengths we calculated form factor F:

$$F = \frac{I + S}{2L} \tag{2}$$

(Wilson and Huang, 1979), elongation e:

$$e = \frac{I}{L} \tag{3}$$

and flatness f:

$$f = \frac{S}{I} \tag{4}$$

(Bagheri and Bonadonna, 2016). We calculated ψ using Equation (1).

For the largest shards we estimated a density of 2456 kg m^{-3}, based on glass composition (Iacovino, 2017; Lange and Carmichael, 1990; Ochs and Lange, 1999). We used the average composition of the rhyolitic component of the Vedde ash from Mangerud *et al.* (1984) and assumed there are no internal bubbles; in reality ~20% of the selected shards contain one or two visible bubbles, but these are small relative to the grain size. The density is consistent with observations by Turney (1998) who extracted the Vedde ash from sediment using liquids with densities of 2400 − 2500 kg m^{-3}.

Dispersion modelling

To test the hypothesis that particle shape is an important factor in distal ash transport we used NAME (Numerical Atmospheric-dispersion Modelling Environment; Jones *et al.* (2007)). NAME is a Lagrangian atmospheric dispersion model, in which model particles are advected by 3D meteorological fields and dispersed using a random walk scheme which includes parameterizations for sub–grid-scale atmospheric

Table 1. Sample codes and locations for samples of the Icelandic Vedde ash used in this study. Latitude and longitude are in decimal degrees (WGS84).

Sample	Latitude	Longitude	Site	Country	Core type	Distance from source (km)	Reference
KV1	63.65914	10.53415	Rørtjønna	Norway	Lake	1454	
KV2	62.02756	5.004157	Kråkenes	Norway	Lake	1232	Mangerud *et al.* (1984); Lohne *et al.* (2014)
KV3	62.52116	6.641243	Stettetjøn	Norway	Bog	1296	Mangerud *et al.* (1984)
KV4	62.48559	6.506024	Slettebakktjønn	Norway	Lake	1291	Mangerud *et al.* (1984)
KV5	62.42842	6.249304	Gjølvatn	Norway	Lake	1280	Mangerud *et al.* (1984)
KV6	62.27965	5.817248	Litletjørn/ Litlevatn	Norway	Lake	1264	Svendsen and Mangerud (1987)
KV7	65.74995	17.89799	Fnjóskadalur	Iceland	Palaeolake	240	Norðdahl and Haflidason (1992)

turbulence and mesoscale motions (Thomson *et al.*, 2009; Webster *et al.*, 2018). NAME also includes parameterizations for wet and dry deposition, with sedimentation schemes for both spherical and non-spherical particles (Webster and Thomson, 2011, 2014; Beckett *et al.*, 2015).

To initialize NAME to model the transport and dispersion of a volcanic ash cloud the following parameters must be provided: source location, eruption start and end times, plume height, source strength (mass eruption rate, MER) and particle characteristics (size, density and shape).

To consider the eruption and meteorological conditions conducive to transport the ash to Norway we first ran a 2D stratified model in MATLAB; full details are given in Supporting Information. This allowed us to test multiple plume height and wind speed scenarios and determine the sensitivity of travel distance to physical particle properties.

We analysed modern meteorological (met) archive data to provide realistic bounds on atmospheric conditions at the time of the Vedde eruption. Single-site met data were obtained from the Wyoming Soundings archive (http://weather.uwyo.edu/upperair/sounding.html). We downloaded soundings from radiosonde ascents for the weather stations at Keflavík, Iceland (site code 04018); Tórshavn, Faroe Islands (06011); and Ørland, Norway (01241; see Fig. 2 for locations), for the period 1973–2018. Data are collected twice daily to measure atmospheric parameters including wind speed, direction, temperature and relative humidity as a function of altitude (<~ 30 km). Monthly average horizontal wind velocities and exceptional records are shown in Fig. 3. In our analysis, we included only single wind speed records containing ≥ 20 discrete height records, with the highest > 25 km. In winter, stratospheric winds over Iceland are generally westerly, with monthly average wind speeds up to ~ 40 m s^{-1} in the stratosphere (Fig. 3; Lacasse, 2001). Several individual records show mean velocities of > 80 m s^{-1} (averaged over 0-25 km).

We found that, assuming a constant wind field in our simple modelling setup, to explain the transport of the largest Vedde ash shards we needed:

- A high plume (> 20 km).
- Wind speeds higher than the stratospheric monthly averages shown in Fig. 3.

Travel distance was more sensitive to size than shape, in agreement with Beckett *et al.* (2015). Uncertainties in particle density translate into differences in travel distances which are small compared to the differences due to size and shape, suggesting our measurement methods are robust. A full description of the model setup, our calculation of uncertainties and their propagation into travel distance is given in the Supporting Information.

We then ran NAME using 3D analysis meteorology from the Unified Model (UM; Cullen, 1993). The UM met data are from 2011 to the present, have a horizontal resolution of between 17 and 25 km, have a temporal resolution of 3 h, and include wind speed and direction as well as other meteorological parameters such as cloud water and ice, precipitation, and boundary layer height (Thomson *et al.*, 2009; Webster and Thomson, 2011; Witham *et al.*, 2017). As our initial sensitivity analysis determined that wind speeds higher than any monthly average were necessary, we used the radiosonde dataset (Fig. 3) to identify dates with favourable conditions for ash transport from Iceland to Norway. Dates (dd/mm/yy) where mean wind speed from 0 to 25 km was > 40 m s^{-1} and the mean wind direction from 0 to 25 km was between 220 and 320o for at least two sites out of three North Atlantic weather stations (Fig. 2) are: 07/03/11, 08/03/11, 23/03/11, 10/03/14, 16/03/14, 26/01/15, 11/02/15 and 28/12/16. NAME runs for these eight dates used UM data from 59 pressure levels to ~ 29 km altitude; the meteorological conditions higher in the stratosphere were taken to be the same as at 29 km. A full description of this 'persisted met' approach is given in the Supporting Information. Particles were released in a uniform distribution from the vent height to the plume top at 35 km agl over an 8-h period from 00:00 to 08:00 h on each day and tracked for 48 h to ensure deposition of at least 99% of the mass released. As we are interested in particle travel distance rather than deposit thickness, we plot deposition as the fraction of total mass in each grid cell, using a minimum contour of 10^{-20}. The chosen MER is therefore arbitrary; we use 2×10^{12} g h^{-1}.

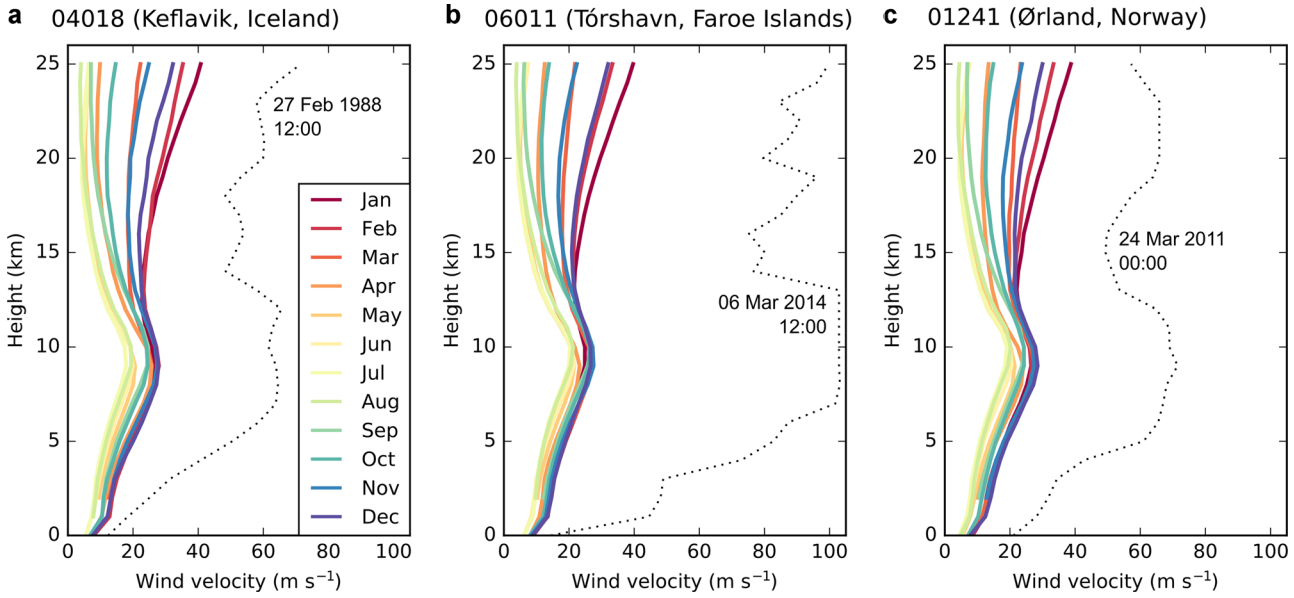

Figure 3. Balloon-borne radiosonde data for the weather stations at (a) Keflavík, Iceland, (b) Tórshavn, Faroe Islands, and (c) Ørland, Norway. Station codes correspond to locations in Fig. 2. Coloured lines show monthly mean speed at each height for the period 1973 - 2018. Dashed lines show individual records for days with extremely high winds, with the day and time chosen based on the highest (height-averaged mean) wind velocities. [Color figure can be viewed at wileyonlinelibrary.com].

Plume height can be constrained using empirical fits to mass eruption rate (Mastin *et al.*, 2009), or maximum clast size in very proximal deposits (within tens of kilometres; Burden *et al.*, 2011) but this is not feasible for the Vedde eruption due to the near-absence of proximal deposits. Maximum plume height estimates for recent Icelandic eruptions range from 10 to 20 km (e.g. Biass *et al.*, 2014; Leadbetter and Hort, 2011), but our initial analysis (Supporting Information) indicated a plume >20 km was needed. Carey *et al.* (2010) estimated a maximum plume height of 34 km for the 1875 explosive eruption of Askja volcano using the method of Carey and Sparks (1986). Sharma *et al.* (2008) estimated a plume height of 30-34 km for the 1362 eruption of Öræfajökull, using maximum clast size data. Both eruptions transported ash to Scandinavia (Pilcher *et al.*, 2005; Carey *et al.*, 2010). Based on these estimates we use 35 km agl as an upper bound.

We calculated terminal velocity w_t using the drag laws of White (1974) for spherical particles and Ganser (1993) for non-spherical particles; full details of the drag laws are given in the Supporting Information. For particle size, we used 191 μm, the d_{v5} of sample KV4, as a maximum; runs with a shape parameter use $\psi = 0.55$, the mean ψ of those particles. We chose sample KV4 as these particles had the highest w_t of the Norwegian samples according to preliminary calculations using Ganser's (1993) drag law, allowing us to constrain the minimum conditions necessary for transport.

Results

Particle size and shape

The Vedde ash sample collected in Iceland, KV7, has a single modal sieve size of 250 − 354 μm with the largest grains > 1 mm; grain sizes in the Norway samples (KV1–6) are smaller (Fig. 4a), as anticipated (e.g. Carey and Sparks, 1986; Folch, 2012). Samples KV1–6 have a single common mode of 45 − 90 μm, despite a range of geographical settings and distances from source (Table 1). Optical microscopy measurements of the size parameters d_{v5} and L_5 are >100 μm in all distal samples, with KV4 having the largest d_{v5} and L_5 of 191 μm and 451 μm, respectively. All data are presented in the Supporting Information.

The standard size parameter for ash dispersal modelling is d_v although L is more commonly measured. L/d_v for samples KV1–6 ranges from 1.7 to 3.3 with a mean of 2.3 (Fig. 4b). In total, 81% of the CT data for the 90 − 125 μm sieve fraction from these samples are in this L/d_v range (contours in Fig. 4b), although the minimum L/d_v is close to 1, the value for a sphere, and the maximum $L/d_v = 10.9$. The range of L/d_v ratios we observe is similar to the range of L/I ratios measured by Mangerud *et al.* (1984) for the Vedde ash.

We obtained bulk shape descriptors from CT scans of the 62.5 − 125 μ m sieve size fraction of each sample (Fig. 5). The proximal and distal samples do not differ significantly in form factor F (Equation (2)), although the Iceland sample has the highest mean F (0.58). Mean flatness f (Equation (4)) and elongation e (Equation (3)) are similar. KV1-5, however, have higher e than f, indicating shards are generally flatter (ratio of short to intermediate axis) than they are elongated (ratio of intermediate to longest axis). Sample KV6, in contrast, has equal mean e and mean f (0.65). Distal samples KV1–6 have flatter shards (mean f of 0.60 − 0.66; Fig. 5c) than proximal sample KV7 (mean $f = 0.74$). Differences between proximal and distal ash are most pronounced in the surface-area–based shape factor sphericity (ψ), which ranges from a mean of $\psi = 0.56$, with 50% of the data between 0.45 and 0.67, in the Iceland sample KV7 to a mean ψ of 0.37 − 0.43 for distal samples KV1–6. Sphericities of larger shards measured by optical microscopy fall within the range of values observed using tomography (Fig. 5a) but are generally higher than the mean. We note that the optical microscopy method approximates particles as smooth flat plates and therefore does not account for small-scale surface roughness measured by CT; in addition, shape can vary with particle size.

Modelled travel distance

Preliminary analysis (Supporting Information) suggested that measuring L_5 could not explain the transport of the largest Vedde shards even assuming extreme idealized conditions (plume height of 35 km and a constant wind speed of 80 m s^{-1} for the entire particle trajectory, which is unlikely). Modelling using NAME confirms the discrepancy in travel distance between runs with L_5 of sample KV4 (451 μm; Fig. 6a,b) and d_{v5} (191 μm; Fig. 6c,d).

Even using d_{v5}, we must model particles as non-spheres using Ganser's (1993) drag law and our measured ψ of 0.55 to explain the transport of the largest Vedde ash shards to Norway. In one NAME simulation using particle size = 191 μm and $\psi = 0.55$ (23/03/11), five of the six sites fall within the great circle distance enclosing 95% of erupted mass deposition (Fig. 6d). For the other dates we modelled, sites KV1–6 fall outside this distance, but the results show that a small amount of mass (< 5%) can travel the distance required for deposition

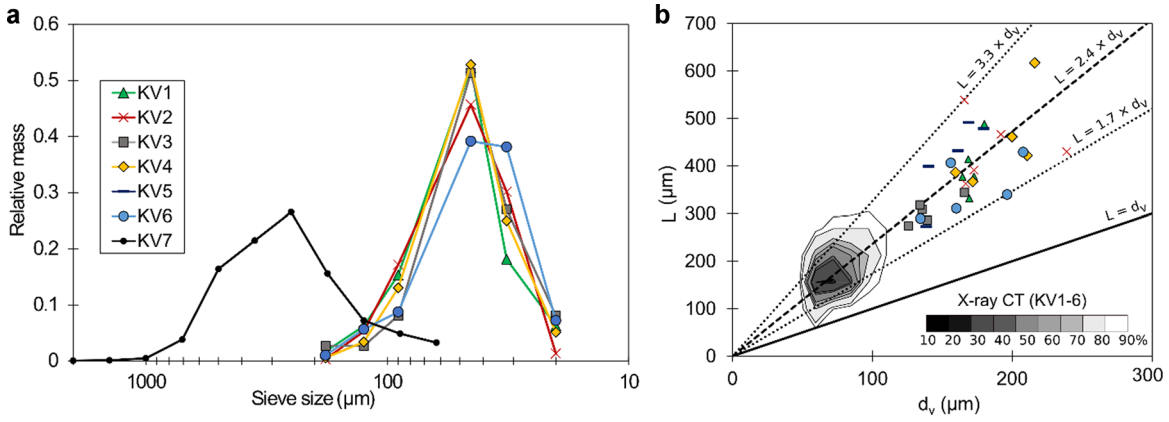

Figure 4. Vedde ash particle size. (a) Sieve size distributions for samples KV1–6 (Norway; excluding KV5 which was sieved to >63 μm prior to this study) and KV7 (Iceland). (b) Particle long axis L and geometric size d_v for the five largest particles in each of the samples KV1–6, measured using optical microscopy. L ranges from 1.7 to 3.3 × d_v. For comparison X-ray CT data from 5241 ash particles are contoured for the same samples. [Color figure can be viewed at wileyonlinelibrary.com].

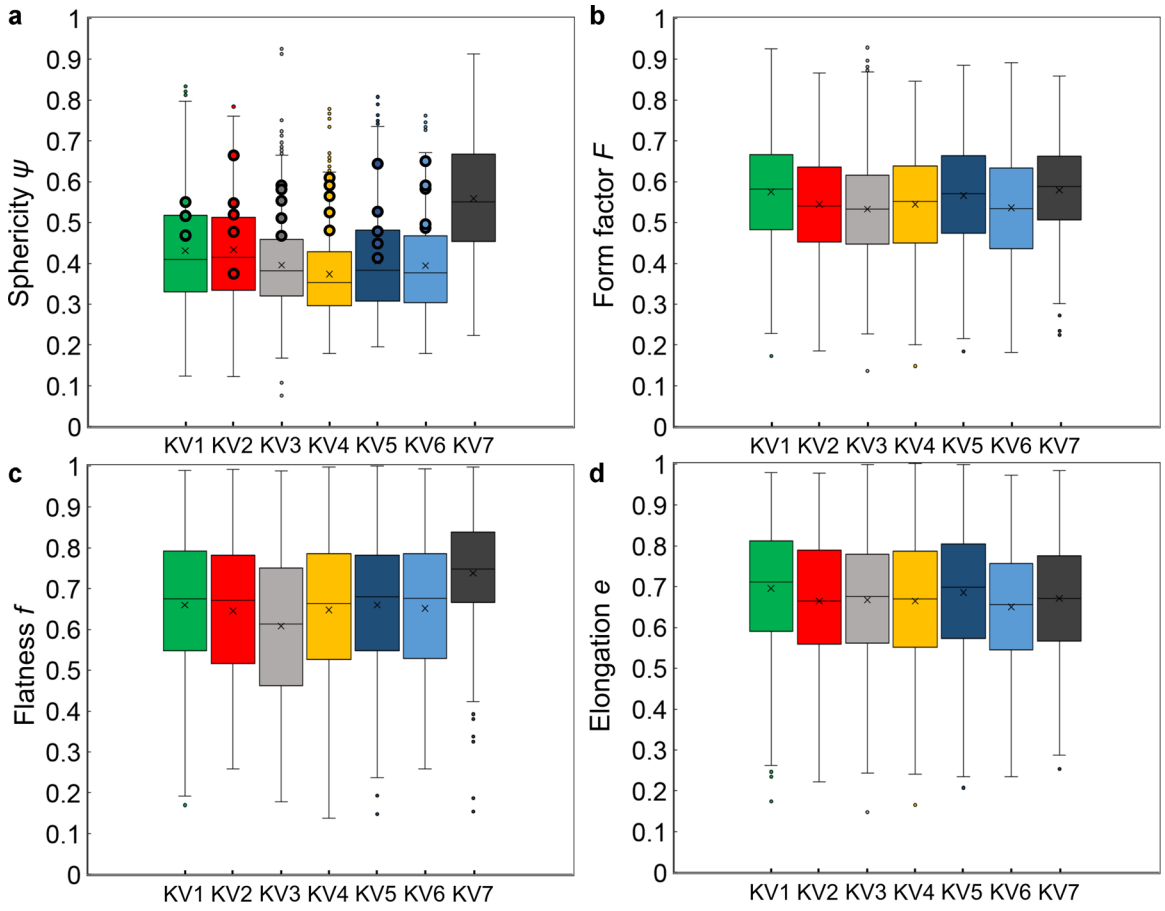

Figure 5. 3D shape data for the 62.5 − 125 μm sieve size fraction, Vedde samples KV1-7, measured using X-ray CT: (a) sphericity ψ (Ganser, 1993), (b) form factor F (Wilson and Huang, 1979), (c) Flatness f (Bagheri and Bonadonna, 2016), and (d) elongation e (Bagheri and Bonadonna, 2016). Crosses indicate the mean value; lines show the median and lower and upper quartiles. For all shape factors, a value of 1 indicates an equant particle (in the case of ψ, a sphere; in the case of e and f, a particle with at least two axes of equal length; for F, three axes of equal length). Small markers show outliers; large markers in plot (a) indicate sphericity of the five largest shards in samples KV1–6 measured using optical microscopy. [Color figure can be viewed at wileyonlinelibrary.com].

in western Norway. Simulations for the other seven days for which we ran NAME are given in the Supporting Information (Supplementary Figures S1-S2; corresponding wind profiles are given in Supplementary Figure S3). In all simulations using spheres with $d_v = 191$ μm, 95% of the mass is deposited within 880 km of the source and no mass travels to the Norwegian sites (minimum distance of 1232 km, Fig. 6c; Supporting Information), indicating that particle shape exerts an important control on distal dispersion of the largest Vedde ash shards.

Modelling transport of the modal size fraction (45 − 90 μm) shows that its maximum travel distance is less sensitive to shape (Fig. 6e,f) than the largest grains, and that deposition of a single size fraction can occur over a wide area.

Cryptotephra sampling strategies

The discrepancy between modelled travel distances of the largest Vedde ash shards for different methods of quantifying size and shape (Fig. 6) illustrates the need for accurate measurements of maximum particle size and shape. Consideration must be given, therefore, to sampling strategy (Bonadonna *et al.*, 2006).

The Norwegian Vedde ash deposits KV1–6 are thicker (Fig. 7a) than other samples collected at a similar distance from the source. Mangerud *et al.* (1984) calculated the original thicknesses in the Ålesund area of western Norway, the location of Vedde samples KV3–5, to be about 2–3 mm (compacted thickness) based on a regression between the lake area to catchment area ratio and the Vedde ash thickness observed; even these corrected thicknesses are anomalous relative to other locations in Scandinavia. The narrow geographical distribution of visible tephra (Fig. 2) suggests that the western Norway Vedde sites could be on-axis (in line with the prevailing wind direction). On-axis transport may also explain the higher maximum shard size of the visible tephra layers (Fig. 7b), where maximum shards are $140 < d_{v5} < 191$ μm and $306 < L_5 < 451$ μm. As western Norway has mountainous topography, orographic effects could also explain the greater fallout of ash in this region (e.g. Watt *et al.*, 2015).

To determine whether the large maximum ash size is a function of the large available sample, we progressively subsampled the X-ray CT dataset for the 62.5 − 125 μm sieve fraction of sample KV3, the largest CT dataset. Our results show that the method of size measurement (L or d_v) has more of an impact on results than the number of particles averaged or the choice of mean or median as an averaging technique (Fig. 8a), in agreement with observations using much coarser proximal tephra deposits (Bonadonna *et al.*, 2006). For example, a sample of > 1000 particles is required to obtain a consistent maximum size d_{v5} (Fig. 8b), which suggests that measurements of maximum shard size are not accurate where only a few shards are available, as in very distal cryptotephra deposits. Accurate calculation of mean size, in contrast, requires only about 50 shards (Fig. 8b).

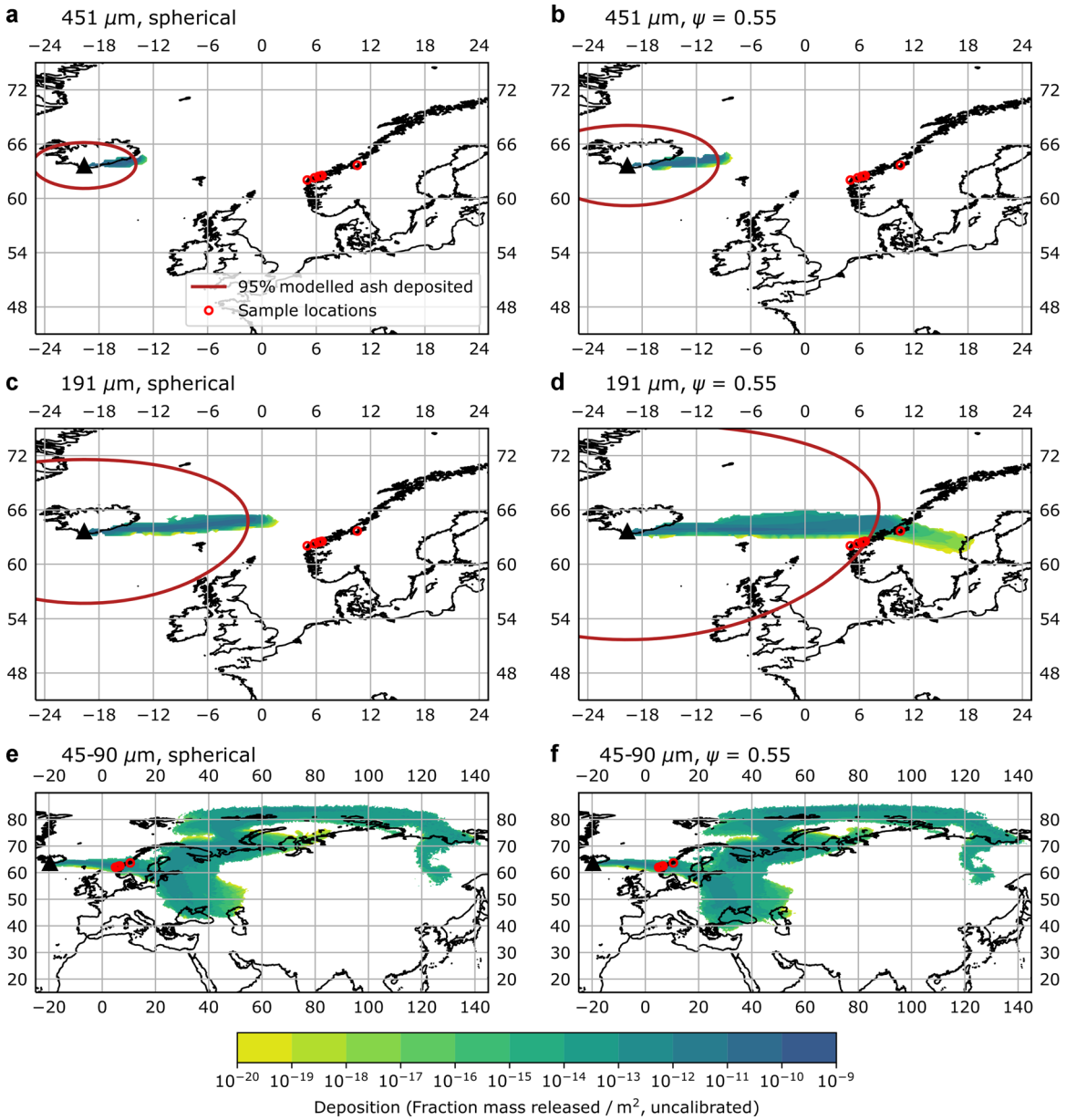

Figure 6. Simulated isomass maps for a Vedde-like eruption of Katla volcano (black triangle) on 23/03/2011 using a 35 km agl plume height. Sample locations are given for sites KV1–6 to provide a reference for observed particle travel distances. The red line indicates the great circle distance from the source at which 95% of the erupted mass has been deposited. In the figure, 451 μm is L_5 of sample KV4; 191 μm is d_{v5} of sample KV4; and 45 − 90 μm is the modal sieve fraction for all western Norway samples. [Color figure can be viewed at wileyonlinelibrary.com].

Discussion

We show that particle shape, and conversion to size, is one of the major contributing factors in the distal transport of the Vedde ash. Importantly, particle shape affects size measurements (e.g. $d_v < L$); our results suggest that the discrepancy in methods of size measurement between the dispersion modelling and cryptotephra communities can explain much of the reported discrepancy between observed and modelled travel distances (Lacasse, 2001; Beckett *et al.*, 2015; Stevenson *et al.*, 2015; Watson *et al.*, 2016).

Quantitative size and shape data for distal tephra are scarce, but are important for understanding eruptions for which proximal data are unavailable (Lane *et al.*, 2012), and for the validation of dispersion models (Witham *et al.*, 2007). Distal Vedde ash samples are not only finer grained but also less spherical on average than the proximal sample: the distal samples have a modal sieve size 45 − 90 μm and mean ψ of 0.37-0.43; the proximal sample has a modal sieve size of 250 − 354 μm and mean $\psi = 0.56$ (sphericity values are for sieve size 62.5 − 125 μm). This indicates that physical particle properties are a strong control on distal tephra dispersion.

The difference in shape between proximal and distal samples is most pronounced when we measure ψ, which may be because ψ, as a surface area-based measure, is sensitive to surface roughness. Proximal and distal samples also differ in flatness f. In contrast, all samples have similar mean values for elongation e and form factor F, suggesting a narrower range of these shape measures produced by fragmentation at source, and/or that flatness and surface roughness have a greater impact on terminal velocity.

The influence of shape and size on travel distance is confirmed by dispersion modelling, by which we can explain the travel distance of the largest grains in Vedde sites KV1–6 only if we quantify size as d_v and model particles as non-spheres with sphericity calculated by Equation (1) and using the drag law of Ganser (1993) (Fig. 6). To be confident in this conclusion also requires

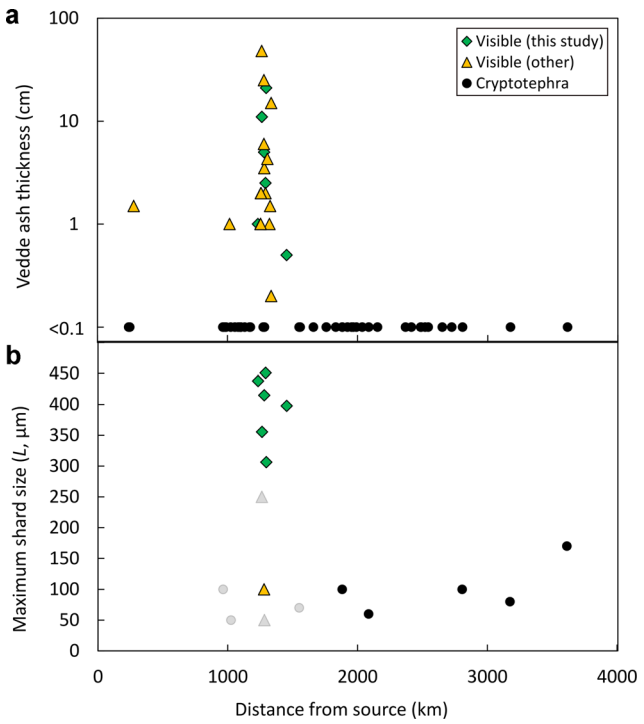

Figure 7. Published measurements of (a) tephra layer thickness and (b) maximum shard size with distance from vent. All data sources are given in the Supporting Information; size data from this study are L_5 and from other studies are L. We include data from studies which do not specify the size parameter measured as greyed out symbols of the same shape. [Color figure can be viewed at wileyonlinelibrary.com].

consideration of uncertainty in the model physics and the associated sensitivity of NAME output. Of six eruption source parameters and 12 internal model parameters, Harvey *et al.* (2018) found that NAME outputs are most sensitive to plume height, MER, the precipitation threshold for wet deposition, and free tropospheric turbulence. We suggest uncertainty due to the model physics is less than the uncertainty in source parameters. The particles we modelled are sufficiently large to be unaffected by turbulence as their terminal velocities are much greater than turbulent vertical velocities (Saxby *et al.*, 2018). We normalize our model results to be independent of MER and take a maximum likely plume height for Icelandic eruptions. Even using a maximum plume height and extreme wind conditions we show that it is necessary to evoke particle non-sphericity to explain transport distance.

Particle size measured for distal deposits has implications for PSDs used to forecast ash concentrations in the atmosphere. Of nine worldwide VAACs (Volcanic Ash Advisory Centres), only one (Buenos Aires) considers particles >100 μm by default for forecasting ash dispersion (Hort, 2016). We show that although the bulk of ash in distal deposits is <100 μm, d_{v5} > 100 μm in all samples (Fig. 4), meaning that particles >100 μm can travel >1000 km from source.

We can explain transport of the largest Vedde ash shards (d_v = 191 μm and ψ = 0.55) to Norway assuming a plume height of 20–35 km agl (Fig. 6). Comparison with minimum eruption volume estimates of 2.8 – 3.3 km^3 (Lacasse *et al.*, 1995) for the marine ash deposit North Atlantic Ash Zone 1 (NAAZ1), which is correlated to the Vedde ash (Lacasse *et al.*, 1996), suggests a Volcanic Explosivity Index (VEI) ≥ 5; eruptions of this magnitude are associated with plumes > 25 km (Newhall and Self, 1982) and so it is reasonable to invoke a high plume for the Vedde eruption.

Modelling results rely on accurate measurement of maximum grain size, which we assume provides constraints on maximum transport distance. The terminal velocity of very fine particles is low compared to atmospheric vertical velocities (advection and diffusion) meaning that travel distance does not strongly depend on their physical properties; the residence time of particles with d_v = 10 μm is insensitive to shape while for particles with d_v = 100 μm it is highly sensitive to shape (Saxby *et al.*, 2018). The exact size at which terminal velocity becomes dominant depends on atmospheric velocities, particle shape and density. The influence of atmospheric velocity partly explains why grains of a single size fraction (45 – 90 μm) can deposit over a range of distances (Fig. 6); this is also due to the vertical spread of ash in the plume and spatial variation in depositional processes such as removal by precipitation (Webster and Thomson, 2014), aggregation (Bagheri *et al.*, 2016), topographic effects (Watt *et al.*, 2015) and gravitational instabilities in the proximal ash cloud (Manzella *et al.*, 2015). Aggregation causes both early fallout of fine particles and delayed sedimentation of larger particles due to coating with finer particles, forming low-density composites in a process known as 'rafting' (Bagheri *et al.*, 2016). All these factors may explain the poor correlation between modal cryptotephra shard size and distance (Watson

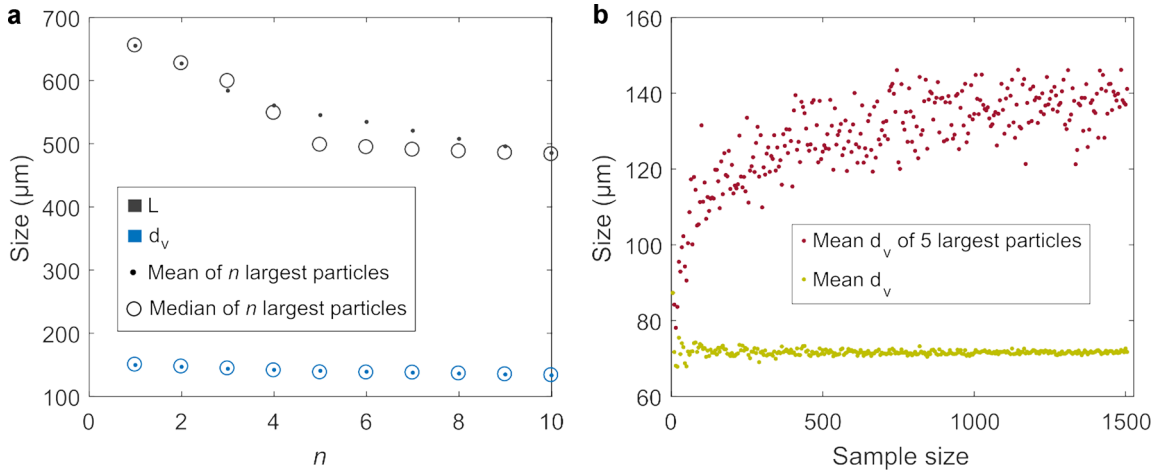

Figure 8. Effect of (a) the size parameter measured, and the averaging technique (mean or median, and the number of largest particles averaged n) on the maximum size observed in a sample of 1507 particles; and (b) by randomly subsampling the same dataset, the effect of sample size on measurement of maximum shard size. Data are for sample KV3; 62.5 – 125 μm sieve fraction. [Color figure can be viewed at wileyonlinelibrary.com].

et al., 2016), and explain why a range of ash particle sizes are found in any given sample location.

We therefore suggest that modelling transport distance as a function of terminal velocity is only meaningful when the largest shards of a sample can be accurately identified, meaning a sample of 500 and ideally > 1000 shards, and those shards have d_{v5} on the order of 100 μm. However, measurements of smaller or fewer shards are useful in other volcanological applications: shard size can inform estimations of total grain size distribution, eruptive style and magnitude (see Cashman and Rust in this issue).

The Vedde ash was selected for this study of the impact of size and shape on travel distance due to its characteristic platy shard morphology (Mangerud *et al.*, 1984) and its abundance in European sediment sequences (Lane *et al.*, 2012). However, it is important to note that the samples are from deposits that have been reworked. Ash particles can undergo sorting by size and shape due to fluvial processes; for example, Watson *et al.* (2016) found that cryptotephra shards were larger in lakes than in neighbouring peat bogs. However, despite differences in deposit thickness and drainage basin size, we find no significant difference in the particle shape and size distributions for the six Norwegian sites studied, suggesting that our observations of shard size and shape are representative of the primary air fall deposit.

We present a method of assessing the transport of ash from an eruption at a time for which no meteorological data are available, by setting upper limits on plume height and wind speed based on modern met data. Tephra may have been able to travel further in the Pleistocene, however, due to stronger atmospheric circulation (Sigurdsson, 1990). Additionally, changes in atmospheric temperature during cold stadials, and the resulting atmospheric density increase, could increase the neutral buoyancy height of the plume (Lacasse, 2001). Our results should therefore be interpreted as maximum possible dispersion distances under ideal modern conditions. Furthermore, controls on tephra transport (e.g. plume height, meteorology) can change during an eruption and so another major assumption in linking ash transport models to deposit characteristics is that all samples are from the same eruptive phase. This is particularly relevant when studying cryptotephra deposits for which the eruption chronology is unknown. The Vedde ash has been tentatively linked to the Sólheimar ignimbrite in Iceland (Lacasse *et al.*, 1995), raising the possibility of additional atmospheric ash injection via a co-ignimbrite plume, which could have been subject to different meteorological conditions. In fact, although our model runs can account for the transport of ash from Iceland to Norway, they cannot account simultaneously for deposition of the Vedde ash to the north and west of the vent (northern Iceland and Greenland; Fig. 2). A change of wind direction during the eruption, or vertical inhomogeneity in the wind field, may be necessary to explain these deposits.

Finally, our results suggest additions to cryptotephra sampling and measuring techniques for volcanological applications. Ideally, maximum shard size should be measured, although this requires a sample of at least 500 and optimally > 1000 shards (Fig. 8). Measurements taken from smaller samples are still useful as the mean shard size can be accurately quantified using fewer (~ 50) shards; the number measured should be noted. Also important is calculation of the size parameter d_v, the parameter most often used in dispersion models; estimates can be obtained rapidly for translucent shards using an optical microscope. It is useful to report particle sphericity ψ where surface area can be measured. For eruptions where ψ is not available, it is reasonable to assume a non-spherical shape (Dunbar *et al.*, 2017). If there is a relationship between maximum shard size, particle shape, and transport distance, as shown here, modelling of cryptotephra transport could be used to estimate eruption parameters (Watson *et al.*, 2016); inverting for plume height (mass eruption rate) and wind speed from proximal deposits is already common (e.g. Carey and Sparks, 1986). Note that plume height and wind speed constraints will be minima because of uncertainties in defining particle size and the modelling assumption that samples are collected on-axis. For most cryptotephra deposits, the plume axis is poorly constrained, and particles are unlikely to have followed the shortest path from source to deposit.

Acknowledgements. This work was supported by NERC and the Met Office, UK, as well as the AXA Research Fund and a Royal Society Wolfson Merit Award (to K. C.). We thank Jan Mangerud, Stefan Wastegård and Simon Larsson for providing the Norwegian Vedde ash samples and for many useful discussions, Sigurður Reynir Gíslason for the Icelandic Vedde ash sample, and Tom Davies for his help with tomography data. We also thank Claire Witham for her feedback on an earlier draft.

Supporting information

Additional supporting information may be found in the online version of this article at the publisher's web-site.

Figure S1: Simulated isomass maps for a Vedde-like eruption of Katla volcano(black triangle), using the NAME model with the Ganser (1993) sedimentationscheme for non-spherical particles, d_v = 191 μm and ψ = 0.55. Sample locations(red circles) are given for sites KV1-6 to provide a reference for observed particletravel distances.

Figure S2: Simulated isomass maps for a Vedde-like eruption of Katla volcano(black triangle), using the NAME model with the White (1974) sedimentationscheme for spherical particles and d_v = 191 μm. Sample locations (red circles)are given for sites KV1-6 to provide a reference for observed particle traveldistances.

Figure S3: Single-site met (radiosonde) data for the days in correspondingpanels of Supplementary Figures S1 - S2. Line colours refer to the weather stationsin the north Atlantic region; their locations are shown in Figure 2.

Figure S4: Sensitivity of NAME modelled volcanic ash air concentrations to thechoice of vertical UM model levels used and the plume height. a) Wind speed in the troposphere and stratosphere for 63.6467°N, 19.1303°W on 2018/12/20,using 70 UM model levels; b) Wind speed persisted above UM model level 59for the same day; the remaining panels are air concentrations two hours after theeruption end, shown as a single contour with a threshold of 0.002 g m-3: c) 25km plume, 70 model levels; d) 25 km plume, 59 model levels; e) 35 km plume,70 model levels; f) 35 km plume, 59 model levels.

Figure S5: Sensitivity of particle travel distances in a stratified atmosphere toaltering the physical particle properties (d = 191 μm or d = 451 μm, and shape= spherical or ψ = 0.55), and transport conditions (plume height H and windvelocity W). For each of the four particles, 112 points are plotted, each for adifferent combination of H and W (see text for full ranges). The inset shows therange of H and W for which particles with d = 191 μm and ψ = 0.55 travelledas far or further than the great circle distance from Katla volcano to sample sites KV1-6 (green shading).

REFERENCES

Bagheri G, Bonadonna C. 2016. On the drag of freely falling non-spherical particles. *Powder Technology* **301**: 526–544.

Bagheri G, Rossi E, Biass S, *et al.* 2016. Timing and nature of volcanic particle clusters based on field and numerical investigations. *Journal of Volcanology and Geothermal Research* **327**: 520–530.

Beckett FM, Witham CS, Hort MC, *et al.* 2015. Sensitivity of dispersion model forecasts of volcanic ash to the physical characteristics of the particles. *Journal of Geophysical Research*.

Biass S, Scaini C, Bonadonna C, *et al.* 2014. A multi-scale risk assessment for tephra fallout and airborne concentration from multiple Icelandic volcanoes - Part 1: Hazard assessment. *Natural Hazards and Earth System Sciences Discussions* **14**(8): 2265–2287.

Blockley SP, Pyne-O'Donnell SD, Lowe JJ, *et al.* 2005. A new and less destructive laboratory procedure for the physical separation of distal glass tephra shards from sediments. *Quaternary Science Reviews* **24**: 1952–1960.

Bonadonna C, Cioni R, Pistolesi M, *et al.*, 2006. *Determination of the largest clasts of tephra deposits for the characterization of explosive volcanic eruptions: IAVCEI Commission on Tephra Hazard Modelling*. Technical report, IAVCEI.

Burden RE, Phillips JC, Hincks TK. 2011. Estimating volcanic plume heights from depositional clast size. *Journal of Geophysical Research: Solid Earth* 116.

Carey RJ, Houghton BF, Thordarson T. 2010. Tephra dispersal and eruption dynamics of wet and dry phases of the 1875 eruption of Askja Volcano. *Bulletin of Volcanology* **72**(3): 259–278.

Carey S, Sparks RS. 1986. Quantitative models of the fallout and dispersal of tephra from volcanic eruption columns. *Bulletin of Volcanology* **48**: 109–125.

Cullen MJP. 1993. The unified forecast/climate model. *Meteorological Magazine* **122**(1449): 81–94.

Dunbar NW, Iverson NA, Van Eaton AR, *et al.* 2017. New Zealand supereruption provides time marker for the Last Glacial Maximum in Antarctica. *Scientific Reports* **7**(1): 12238.

Folch A. 2012. A review of tephra transport and dispersal models: Evolution, current status, and future perspectives. *Journal of Volcanology and Geothermal Research* **235-236**: 96–115.

Ganser GH. 1993. A rational approach to drag prediction of spherical and nonspherical particles. *Powder Technology* **77**: 143–152.

Haflidason H, Regnéll C, Pyne-O'Donnell S, *et al.* 2018. Extending the known distribution of the Vedde Ash into Siberia: occurrence in lake sediments from the Timan Ridge and the Ural Mountains, Northern Russia. *Boreas* **48**(2): 444–451.

Harvey NJ, Huntley N, Dacre H, *et al.* 2018. Multi-level emulation of a volcanic ash transport and dispersion model to quantify sensitivity to uncertain parameters. *Natural Hazards and Earth System Sciences* **18**(1): 41–63.

Hort MC 2016. *VAAC operational dispersion model configuration snap shot Version 2*. Technical Report March, NCEP, Washington.

Iacovino K 2017. Glass Density Calc v3.2.

Ingólfsson Ó, Norðdahl H. 2010. 4 Deglaciation and Holocene Glacial History of Iceland. *Developments in Quaternary Sciences* **13**: 51–68.

Jones A, Thomson D, Hort M, *et al.* 2007. The U.K. Met Office's next-generation atmospheric dispersion model, NAME III. In *Air Pollution Modeling and Its Application XVII*, Borrego C, Norman A-L (eds). Springer: Boston; 580–589.

Lacasse C. 2001. Influence of climate variability on the atmospheric transport of Icelandic tephra in the subpolar North Atlantic. *Global and Planetary Change* **29**(1-2): 31–55.

Lacasse C, Sigurdsson H, Carey S, *et al.* 1996. North Atlantic deep-sea sedimentation of Late Quaternary tephra from the Iceland hotspot. *Marine Geology* **129**(3-4): 207–235.

Lacasse C, Sigurdsson H, Jóhannesson H, *et al.* 1995. Source of Ash Zone 1 in the North Atlantic. *Bulletin of Volcanology* **57**(1): 18–32.

Lacasse C, van den Bogaard P. 2002. Enhanced airborne dispersal of silicic tephras during the onset of Northern Hemisphere glaciations, from 6 to 0 Ma records of explosive volcanism and climate change in the subpolar North Atlantic. *Geology* **30**(7): 623–626.

Lane CS, Blockley SP, Mangerud J, *et al.* 2012. Was the 12.1ka Icelandic Vedde Ash one of a kind? *Quaternary Science Reviews* **33**(February): 87–99.

Lange AR, Carmichael ISE. 1990. Thermodynamic properties of silicate liquids with emphasis on density, thermal expansion and compressibility. *Modern Methods of Igneous Petrology: Understanding Magmatic Processes* **24**: 25–64.

Lawson IT, Swindles GT, Plunkett G, *et al.* 2012. The spatial distribution of Holocene cryptotephras in north-west Europe since 7 ka: Implications for understanding ash fall events from Icelandic eruptions. *Quaternary Science Reviews* **41**: 57–66.

Leadbetter SJ, Hort MC. 2011. Volcanic ash hazard climatology for an eruption of Hekla Volcano, Iceland. *Journal of Volcanology and Geothermal Research* **199**(3-4): 230–241.

Lohne ØS, Mangerud J, Birks HH. 2014. IntCal13 calibrated ages of the Vedde and Saksunarvatn ashes and the Younger Dryas boundaries from Kråkenes, western Norway. *Journal of Quaternary Science* **29**(5): 506–507.

Mangerud J, Lie SE, Furnes H, *et al.* 1984. A Younger Dryas ash bed in western Norway, and its possible correlations with tephra in cores from the Norwegian Sea and the North Atlantic. *Quaternary Research* **21**: 85–104.

Manzella I, Bonadonna C, Phillips JC, *et al.* 2015. The role of gravitational instabilities in deposition of volcanic ash. *Geology* **43**(3): 211–214.

Mastin LG, Guffanti M, Servranckx R, *et al.* 2009. A multidisciplinary effort to assign realistic source parameters to models of volcanic ash-cloud transport and dispersion during eruptions. *Journal of Volcanology and Geothermal Research* **186**: 10–21.

Mele D, Dioguardi F. 2018. The grain size dependency of vesicular particle shapes strongly affects the drag of particles. First results from microtomography investigations of Campi Flegrei fallout deposits. *Journal of Volcanology and Geothermal Research* **353**: 18–24. https://doi.org/10.1016/j.jvolgeores.2018.01.023

Newhall CG, Self S. 1982. The volcanic explosivity index (VEI): An estimate of explosive magnitude for historical volcanism. *Journal of Geophysical Research* **87**(C2): 1231–1238.

Norðdahl H, Haflidason H. 1992. The Skógar Tephra, a Younger Dryas marker in North Iceland. *Boreas* **21**: 23–41.

Ochs FA, Lange RA. 1999. The density of hydrous magmatic liquids. *Science* **283**: 1314–1317.

Pilcher J, Bradley RS, Francus P, *et al.* 2005. A Holocene tephra record from the Lofoten Islands, Arctic Norway. *Boreas* **34**: 1–21.

Ponomareva V, Portnyagin M, Davies SM. 2015. Tephra without borders: far-reaching clues into past explosive eruptions. *Frontiers in Earth Science* **3**.

Rasmussen SO, Vinther BM, Clausen HB, *et al.* 2007. Early Holocene climate oscillations recorded in three Greenland ice cores. *Journal of Quaternary Science* **26**(15-16): 1907–1914.

Riley CM, Rose WI, Bluth GJS. 2003. Quantitative shape measurements of distal volcanic ash. *Journal of Geophysical Research: Solid Earth* **108**(B10): 1–15.

Rodger H. 2018. *An Investigation of Methods to Obtain 3D and 2D Physical Particle Parameters of Volcanic Ash Grains Which Could Affect Settling Velocity*. PhD thesis, University of Bristol.

Rose WI, Durant AJ. 2009. Fine ash content of explosive eruptions. *Journal of Volcanology and Geothermal Research* **186**: 32–39.

Saxby J, Beckett F, Cashman K, *et al.* 2018. The impact of particle shape on fall velocity: Implications for volcanic ash dispersion modelling. *Journal of Volcanology and Geothermal Research* **362**.

Sharma K, Self S, Blake S, *et al.* 2008. The AD 1362 Öræfajökull eruption, S.E. Iceland: Physical volcanology and volatile release. *Journal of Volcanology and Geothermal Research* **178**(4): 719–739.

Sigurdsson H. 1990. Assessment of the atmospheric impact of volcanic eruptions. *Global catastrophes in Earth history; An interdisciplinary conference on impacts, volcanism, and mass mortality; Geological Society of America Special Paper*, **247**, 99-110.

Stevenson JA, Loughlin S, Rae C, *et al.* 2010. Distal deposition of tephra from the Eyjafjallajökull 2010 summit eruption. *Journal of Geophysical Research* **117**(6).

Stevenson JA, Loughlin SC, Font A, *et al.* 2013. UK monitoring and deposition of tephra from the May 2011 eruption of Grímsvötn, Iceland. *Journal of Applied Volcanology* **2**(3).

Stevenson JA, Millington SC, Beckett FM, *et al.* 2015. Big grains go far: Understanding the discrepancy between tephrochronology and

satellite infrared measurements of volcanic ash. *Atmospheric Measurement Techniques* **8**(5): 2069–2091.

Svendsen JI, Mangerud J. 1987. Late Weichselian and Holocene sea-level history for a cross-section of western Norway. *Journal of Quaternary Science* **2**: 113–132.

Thomson DJ, Jones AR, Webster HN, 2009. *NAME Technical Specification Document C01: Physical and mathematical constants and functions*. Technical report, Met Office, UK.

Tomlinson EL, Smith VC, Albert PG, *et al.* 2015. The major and trace element glass compositions of the productive Mediterranean volcanic sources: Tools for correlating distal tephra layers in and around Europe. *Quaternary Science Reviews* **118**: 48–66.

Turney CS. 1998. Extraction of rhyolitic component of Vedde microtephra from minerogenic lake sediments. *Journal of Paleolimnology* **19**(2): 199–206.

Wastegård S. 2002. Early to middle Holocene silicic tephra horizons from the Katla volcanic system, Iceland: New results from the Faroe Islands. *Journal of Quaternary Science* **17**(8): 723–730.

Watson EJ, Swindles GT, Stevenson JA, *et al.* 2016. The transport of Icelandic volcanic ash: Insights from northern European cryptotephra records. *Journal of Geophysical Research: Solid Earth* **121**: 7177–7192.

Watt SF, Gilbert JS, Folch A, *et al.* 2015. An example of enhanced tephra deposition driven by topographically induced atmospheric turbulence. *Bulletin of Volcanology* **77**(35).

Webster HN, Thomson DJ. 2011. Dry deposition modelling in a Lagrangian dispersion model. *International Journal of Environment and Pollution* **47**(1-4): 1–9.

Webster HN, Thomson DJ, 2014. *Forecasting Research Technical Report No. 584: The NAME wet deposition scheme*. Technical report, Met Office, UK.

Webster HN, Whitehead T, Thomson DJ, *et al.* 2018. Parameterizing unresolved mesoscale motions in atmospheric dispersion models. *Journal of Applied Meteorology and Climatology* **57**(3): 645–657.

White FM. 1974. *Viscous Fluid Flow*. McGraw-Hill: New York.

Wilson L, Huang TC. 1979. The influence of shape on the atmospheric settling velocity of volcanic ash particles. *Earth and Planetary Science Letters* **44**(2): 311–324.

Witham C, Hort M, Thomson D, *et al.* 2017.*Technical Summary (v1.4): The current volcanic ash modelling set- up at the London VAAC*. Technical report, Met Office, UK.

Witham CS, Hort MC, Potts R, *et al.* 2007. Comparison of VAAC atmospheric dispersion models using the 1 November 2004 Grímsvötn eruption. *Meteorological Applications* **14**: 27–38.

